J Soils Sediments (2012) 12:97–114
DOI 10.1007/s11368-011-0402-z

Iron oxide mineralogy and stable iron isotope composition in a Gleysol with petrogleyic properties

Tim Mansfeldt · Stephan Schuth · Werner Häusler · Friedrich E. Wagner · Stephan Kaufhold · Mark Overesch

Received: 28 April 2011 / Accepted: 16 July 2011 / Published online: 5 August 2011

Abstract
Purpose Properties of Fe oxides are poorly understood in soils with fluctuating water tables and variable redox conditions. The objective of this research was to (a) characterize the mineralogical composition of Fe oxides and (b) determine the relationship to the stable Fe isotope ratio in a soil with temporally and spatially sharp redox gradients.

Materials and methods The lowland Gleysol (Petrogleyic) is in Northwest Germany and consists of oximorphic soil horizons (Ah 0–15, Bg 15–35, and CrBg 35–70 cm) developed from Holocene fluvial loam overlaying glacio-fluvial sand with reductomorphic properties (2Cr horizon, +70 cm). Field measurements during the course of 28 months included the monitoring of groundwater table, soil redox potential, and analysis of the soil solutions. Solid Fe phases were studied by room temperature and cryogenic ^{57}Fe Mössbauer spectroscopy, and stable Fe isotope compositions by multiple collector inductively coupled plasma mass spectrometry.

Results and discussion The groundwater table ranged from −83 cm below to +8 cm above soil surface (median −27 cm). Permanent reducing conditions occurred in the 2Cr horizon with dissolved Fe concentrations of 44.8 mg L^{-1} (median). The duration of oxidizing conditions increased in the order CrBg < Bg < Ah. Total Fe increased from 50 (Ah) over 316 (Bg) up to 412 g kg^{-1} (CrBg) and was lowest in the 2Cr horizon (7 g kg^{-1}). Ferrihydrite (51% of total Fe) was dominant over goethite (24%) in the Ah horizon. Conversely, nanogoethite dominated both the Bg (94%) and CrBg (86%) horizons. Iron in siderite amounted to 7% in the CrBg horizon. Iron isotope compositions yielded a range of δ^{57}Fe values from +0.29‰ (Ah horizon) to −0.30‰ (Bg horizon). In contrast to the overlying CrBg (δ^{57}Fe=−0.19‰) and Bg horizons, the 2Cr horizon is characterized by a relatively high δ^{57}Fe value of +0.22‰.

Conclusions Lasting water saturation and frequent reducing conditions lead to the enrichment of goethite in subsoil. Once formed, goethite remains stable compared to ferrihydrite because it is less available for microbial mediated reductive dissolution. High δ^{57}Fe values in the topsoil primary result from fast ferrihydrite precipitation during aeration immediately after reducing conditions. In contrast,

Responsible editor: Michael Kersten

T. Mansfeldt (✉) · S. Schuth · M. Overesch
Department of Geosciences, Soil Geography/Soil Science,
University of Cologne,
Albertus-Magnus-Platz,
50923 Köln, Germany
e-mail: tim.mansfeldt@uni-koeln.de

S. Schuth
Institute of Mineralogy, Leibniz University Hannover,
Callinstraße 3,
30167 Hannover, Germany

W. Häusler
Soil Science, Technical University of Munich,
Am Hochanger 2,
85354 Freising, Germany

F. E. Wagner
Physics Department E15, Technical University of Munich,
85747 Garching, Germany

S. Kaufhold
Federal Institute for Geosciences and Natural Resources (BGR),
Stilleweg 2,
30655 Hannover, Germany

M. Overesch
M&O, Büro für Geowissenschaften,
Südstraße 26b,
49751 Sögel, Germany

the low δ^{57}Fe values of the Fe-rich horizons (Bg, CrBg) promote adsorption of dissolved Fe with a light isotope composition onto goethite during capillary rise. The high δ^{57}Fe value of the Fe-poor subsoil (2Cr) is related to silicate-bound Fe rather than dissolution and precipitation of Fe oxides.

Keywords Iron oxides · Mössbauer spectroscopy · Redox processes · Soil · Stable iron isotopes

1 Introduction

High groundwater tables are a common feature of lowlands and result in frequent water saturation of associated soils. As a result of wet conditions, the diffusion of oxygen (O_2) into soils is extremely impaired. Depending on microbial activity, O_2 supplies are more or less quickly exhausted and soil conditions change from oxidizing to reducing. In the absence of O_2, the oxidized form of Fe (ferric iron or Fe^{III}) acts as one of the most important terminal electron acceptors because microorganisms transfer electrons obtained during metabolic oxidation of organic matter towards Fe^{III} (e.g., Konhauser 2007; Weber et al. 2006). The main pool of Fe^{III} consists of the various forms of Fe oxides, hydroxides and oxyhydroxides (e.g., Cornell and Schwertmann 2003), which will be designated as Fe oxides in the following text. The reduction of Fe^{III} results in the release of reduced Fe, i.e., ferrous iron or Fe^{II} (Weber et al. 2006). Under reducing conditions and acidic to neutral pH, the latter is present as water soluble Fe^{2+}. Upon reintroduction of O_2 into lowland soils, e.g., when water tables are falling, Fe^{2+} is rapidly oxidized, resulting in the simultaneous precipitation as Fe oxide.

Typical mineral soils of lowlands are Gleysols which are characterized by a gleyic color pattern (WRB and IUSS Working Group 2006). While the permanently water-saturated subsurface soil horizons exhibit strongly reducing conditions and consequently *reductomorphic properties*, i.e., Fe oxides are virtually absent and the color is light gray in sandy soils, the overlaying surface horizons reveal *oximorphic properties*. These properties consist of reddish brown to bright yellowish brown mottles arising from the enrichment of different Fe oxides (Cornu et al. 2009; Golden et al. 1997). Overall, the process leading to redox depletion and enrichment zones is termed as *redoximorphosis* (Cornell and Schwertmann 2003). Oximorphic soil horizons are often influenced by stronger fluctuations in groundwater table and capillary fringe. As a result, pronounced short-term fluctuations in soil E_H may occur, encompassing up to several hundred mV (Fiedler et al. 2007; Mansfeldt 2003). Such redox conditions induce a continuous dissolution and re-formation of Fe oxides in oximorphic soil horizons.

Traditionally, Fe oxides in soils have been quantified by selective chemical extractions. The most common procedure to extract the so-called reactive Fe oxides is the use of ammonium oxalate at pH 3 (Schwertmann 1964). Oxalate-extractable Fe (Fe_o) represents poorly crystalline Fe oxides which are nowadays denoted as short-range-ordered oxides. Ferrihydrite (e.g., $Fe_5HO_8{\cdot}4H_2O$) is the most prominent one. The total amount of Fe oxides is obtained by the extraction with a solution of dithionite–citrate–bicarbonate (Fe_d) at 80°C (Mehra and Jackson 1960) that dissolves also crystalline forms of Fe oxides, e.g., goethite (α-FeOOH) or hematite (α-Fe_2O_3). Various soil types and horizons are characterized by distinct ranges in the ratio of oxalate-extractable Fe to dithionite-extractable Fe (Fe_o/Fe_d), reflecting the different environmental conditions (e.g., temperature, redox conditions, presence of organic ligands) under which the Fe oxides have been precipitated and transformed (Blume and Schwertmann 1969; Shaw et al. 2003).

Little work was carried out on the mineralogy of Fe oxides in soils subjected to alternating oxic and anoxic conditions. Sah et al. (1989) inferred that repeated periods of flooding and draining, respectively, increased the precipitation of Fe as oxalate-extractable Fe oxides. However, selective chemical extractions of Fe are not mineral specific. Therefore, their significance is limited. By using Mössbauer spectroscopy, nanocrystalline goethite was found rather than the assumed ferrihydrite in lacustrine and marine sediments (van der Zee et al. 2003). Thompson et al. (2006) demonstrated that nanocrystalline goethite was transformed into microcrystalline hematite and goethite as a result of frequent soil redox fluctuations in Hawaiian topsoil. They did not observe the accumulation of short-range-ordered Fe oxides as expected. However, the cumulative and long-term effects of such redox cycling on Fe oxides and their properties are not well understood. Iron oxides are not only important for the genesis and classification of soils but also for the biogeochemical cycling of many elements. They act, for instance, as a strong adsorbent for toxic (semi)metals like arsenic (Bowell 1994; Herbel and Fendorf 2006) or for nutrients like phosphate (Patrick and Khalid 1974; Peretyazhko and Sposito 2005). Moreover, they are involved in the sequestration of organic carbon (Eusterhues et al. 2011; Kiem and Kögel-Knabner 2002). In this regard, a comprehensive understanding of the properties of Fe oxides is crucial.

Frequent changes of the soil redox conditions affect not only the amount and mineralogical composition of Fe oxides as outlined above but also the relative abundance of stable Fe isotopes because reductive dissolution and precipitation are combined with a significant isotope fractionation of Fe. Upon formation of Fe oxides, the heavy Fe isotopes will enter the crystal lattice preferentially in regard to ^{54}Fe, as described as a general process in the

classical work of Bigeleisen (1965), calculated for Fe compounds by Schauble et al. (2001), and experimentally demonstrated by, e.g., Bullen et al. (2001). For the reverse process (i.e., dissolution of Fe oxides during reducing conditions or weathering of Fe bearing minerals), the light Fe isotopes will enter the solution predominantly (e.g., Brantley et al. 2001; Crosby et al. 2005; Fantle and DePaolo 2004; Staubwasser et al. 2006; Wiederhold et al. 2007a). Other important processes of Fe isotope fractionation are the adsorption of heavy Fe isotopes onto the surfaces of Fe oxides like goethite (e.g., Beard et al. 2010; Icopini et al. 2004; Jang et al. 2008; Mikutta et al. 2009) and slow mineral transformations, e.g., of ferrrihydrite to goethite or siderite to goethite (Clayton et al. 2005; Wiesli et al. 2004). Moreover, bacteria that reduce Fe^{III} to gain energy (e.g., Beard et al. 1999, 2003; Brantley et al. 2001, 2004; Crosby et al. 2005; Icopini et al. 2004) or oxidize Fe^{II} (e.g., Croal et al. 2004; Kappler et al. 2010) have been shown to fractionate Fe isotopes during the process of reduction and oxidation, respectively. Here, the heavy Fe isotopes are being incorporated preferentially by the bacteria, leaving an isotopically light aqueous solution and a comparatively heavy soil horizon behind (e.g., Wiederhold et al. 2007b). With this in mind, soils like Gleysols offer a well-suited natural laboratory to study both the effects of biological activity and changing redox conditions on the mobility and mineral (trans)formation of Fe oxides. Hence, analyses of the four stable Fe isotopes, ^{54}Fe (natural abundance of 5.84%), ^{56}Fe (91.76%), ^{57}Fe (2.12%), and ^{58}Fe (0.28%), should provide a valuable tool to investigate the fate of Fe in soils with strong redox gradients.

The objective of this research was (a) to characterize the mineralogy of Fe oxides and (b) to determine the relationship to the stable Fe isotope composition in a Gleysol with strongly fluctuating redox conditions and massive Fe enrichments. From the above mentioned findings we postulate that even in soil horizons with lasting reducing conditions well crystalline Fe oxides may be present in significant amounts. To obtain information on the solid Fe species, powder X-ray diffraction (XRD), Fourier transform infrared spectroscopy (FTIR), and Mössbauer spectroscopy were employed. Stable Fe isotope compositions were determined by multiple collector inductively coupled plasma mass spectrometry (MC-ICP-MS). Additionally, we present field data of the investigated site to show that the process of redoximorphosis is a rather recent one.

2 Materials and methods

2.1 Study site

Field studies and sampling were carried out at a flat grassland site (the Heubach plain) near Lavesum in the district of Recklinghausen, North Rhine-Westphalia, Germany (51°48′59″ N, 7°12′59″ E). The mean annual precipitation is 783 mm and the mean annual air temperature 9.6°C. Groundwater emerges in this lowland area typically at low depths.

2.2 Field monitoring program

In an area of 3×3 m, groundwater level, soil temperature, and soil redox potential (E_H) were monitored at hourly intervals from August 2006 to June 2008 using a data logger system. The groundwater table was measured by a gauge in a well. Redox potentials were monitored in genetic soil horizons at 10, 30, 50, and 120 cm depth in threefold replication using permanently installed Pt electrodes (Mansfeldt 2003). An Ag-AgCl reference electrode was installed in a salt bridge in the middle of the measuring plot. In the following all redox values are expressed by reference to the standard hydrogen electrode by adding 207 mV. Additionally, E_H was converted into values corresponding to pH 7 (E_H (pH 7)) by Eq. 1 using pH of field-collected soil solutions.

$$E_H(\text{pH } 7) = E_H + (\text{pH} - 7) \times 59, [E_H \text{ in mV}] \quad (1)$$

Soil temperatures were recorded by thermocouples. Soil solutions were collected in the corresponding soil depths with polyamide/polyethylene suction cups (0.45 μm) at low-pressure of about 500 hPa in threefold over a period of 10 to 18 h. Solutions were divided during sampling into two subsamples via Y-junctions installed behind the suction cups. One subsample was collected in a bottle containing an EDTA solution (1 to 3 g L^{-1} EDTA, Titriplex III) in order to prevent any oxidation of Mn and Fe and their subsequent precipitation as oxides. The other subsample was not treated with additives. To minimize contact with air, these subsamples were decanted in the field in smaller bottles, thus ensuring that no headspace exists. After collection, all samples were passed through a 0.45-μm filter and stored at 5°C in opaque glass bottles. Soil solutions with EDTA were analyzed for total dissolved Fe and Mn by flame atomic absorption spectrometry (F-AAS) using an air–acetylene flame with an AAS 3100 instrument (PerkinElmer). Soil solutions without EDTA were analyzed for pH potentiometrically by a glass electrode, and for dissolved inorganic carbon and dissolved organic carbon by acid digestion or thermal combustion prior to infrared CO_2 detection in a TOC/TN_b-analyzer (liquiTOC, Elementar).

2.3 Soil sampling and soil characterization

Soil samples were collected during the summer of 2005 with the water table being 85 cm below surface in a 1.3-m-deep pit from three genetic soil horizons (Ah, Bg, CrBg, about 20 kg

each). The samples were loaded into glass vessels which had been filled previously with solid CO_2 to keep the sample frozen. In the laboratory, they were freeze-dried and sieved (<2 mm). Particle-size distribution was determined by wet sieving and sedimentation using the pipette sampling technique. Soil pH was measured potentiometrically in 0.01 M $CaCl_2$ (soil/solution=1:5 *v/v*). For analysis of total element contents, subsamples were ground in an agate mill. Total C and N were measured by dry combustion with a CNS-Analyser (Vario EL, Elementar). Inorganic C was determined by dry combustion at 1,200°C after adding perchloric acid (15%) to the preheated (60°C) sample using an elemental analyzer (Deltronik, Düsseldorf). The CO_2 evolved was absorbed in an alkaline solution and detected by Coulomb electrochemical titration. Organic C was calculated as the difference between total and inorganic C. Total contents of Fe and Mn were measured by F-AAS in extracts obtained by microwave induced aqua regia digestion.

2.4 Wet chemical Fe oxide analyses

Oxalate-extractable Fe was determined according to Schwertmann (1964) and dithionite-extractable Fe according to Mehra and Jackson (1960). Due to high contents of Fe oxides and the presence of concretions in the soil, soil/solution ratios were changed from 1:50 (oxalate) and 1:25 (dithionite) to 1:500 and 1:250. In addition, ground soil was used instead of sieved soil. Iron and Mn in the extracts were measured by F-AAS.

2.5 Random powder X-ray diffraction

The samples used for X-ray diffraction and Mössbauer spectroscopy were ground with acetone to smaller than 63 μm. The XRD patterns were recorded with a Co radiation source using a Philips PW1070 diffractometer equipped with a graphite monochromator at Technical University of Munich, Germany (Soil Science). A Co source instead of Fe or Cu was used in this study because of the lower absorption of the Co Kα radiation by Fe-rich phases in the samples. The random powder samples were measured from 5 to 80°2Θ in steps of 0.02°2Θ with a counting time of 5 s for each step. For detailed evaluation of the XRD patterns, the single-peak fitting program MacClayFit (Stanjek and Häusler 2000) was used. Natural quartz present in the samples was taken as an internal standard to correct the °2Θ position of each fitted peak.

2.6 Fourier transform infrared spectroscopy

By infrared (IR) spectroscopy minerals can be analyzed by the intensity and position of IR absorption bands. The IR spectroscopy is not suitable for a complete mineralogical assessment, because of similarities in the spectra of the silicates (band coincidences). However, some minerals show characteristic mid-IR absorption bands which can be used as complementary tool particularly for the identification of kaolinite, halloysite, carbonates, quartz, and some Fe oxides. For measuring mid-infrared (MIR) spectra, the KBr pellet technique (1 mg sample/200 mg KBr) was applied. Spectra were collected on a Thermo Nicolet Nexus FTIR spectrometer (MIR beam splitter: KBr, detector DTGS TEC) with a resolution of 2 cm^{-1}. Background corrections were performed with the automatic tool of the Thermo Nicolet software Omnic®. The spectra were acquired at BGR, Hannover (Germany).

2.7 Mössbauer spectroscopy

Mössbauer spectra were measured in transmission geometry with a standard electromechanical spectrometer using a sinusoidal velocity waveform and a source of ^{57}Co in rhodium. The 14.4-keV γ-rays were detected with a Kr proportional counter with single channel analyzer windows set on both the 14.4-keV photo peak and the escape peak. In addition to measurements at ambient temperature (295 K), spectra were recorded at 4.2 K in a liquid He bath cryostat, and measurements at 165 K were performed in the same cryostat with only the radiation shield cooled with liquid nitrogen. During all measurements the source and the absorber were at the same temperature. Absorber thicknesses were 100 mg cm^{-2} for the Ah horizon and 50 mg cm^{-2} for the Bg and CrBg horizons. Absorber thicknesses were 100 mg cm^{-2} for the Ah horizon, and 50 mg cm^{-2} for the Bg and CrBg horizons. The spectra were acquired at the Physics Department of the Technical University of Munich, Germany.

The raw data were folded to eliminate the geometry effect, and then least-squares fitted with one or more appropriate sets of Lorentzian lines or, wherever necessary, with line shapes corresponding to Gaussian distributions of hyperfine fields or electric quadrupole interactions. The Lorentzian line width at half maximum in these distributions was always assumed to be 0.25 mm s^{-1}. Further details will be given below together with the results.

All isomer shifts are given as measured, i.e., with respect to the $^{57}Co/Rh$ source having the same temperature as the absorber, which practically eliminates contributions from the second order Doppler shift. To convert these shifts to shifts with respect to Fe metal having the temperature of the absorber, one has to add 0.11 mm s^{-1}. Since the resonant fractions of the individual phases present in the samples will not differ largely, the relative areas (RA) of the individual components in the Mössbauer spectra can be considered as representing the amounts of Fe in the respective phases to a good approximation.

2.8 Stable iron isotopes

About 100 to 150 mg of powder ground in an agate mill from the dried and sieved samples were digested in HNO_3, HCl, and HF (2:2:1) after treatment with HNO_3 and H_2O_2 (Merck Suprapure®) to destroy organic matter. After digestion, three dry-down steps with HNO_3 followed to remove fluoride compounds. Separation of Fe from the matrix was performed as described by Schoenberg and von Blanckenburg (2005), using ~1.5 mL of an anion exchange resin (Bio-Rad® AG1 X8, 100–200 mesh). All acids were cleaned in teflon distills at sub-boiling conditions before use. The separation process was repeated once to ensure a clean Fe fraction. The average total analytical blank was ~9 ng Fe which is negligible relative to the amounts of ~1 to 3 mg Fe loaded onto the columns. Final yields always exceeded 98% of total Fe.

In order to further distinguish between silicate- and oxide-bound Fe isotope compositions, we analyzed in duplicate the Fe isotopes of dithionite-extractable Fe (Fe_d) and the residue after Fe_d extraction of the Ah and the 2Cr horizon, respectively. For the Bg and CrBg horizon, most Fe is bound as oxide (Table 3) which was analyzed after total digestion (see above). The Fe-complexing dithionite–citrate–bicarbonate reagent used for extraction was destroyed by following the protocol of Staubwasser et al. (2006) before application of the anion exchange resin procedure. Quantitative Fe separation is essential to avoid any artificial isotope fractionation. The residue after Fe_d extraction was washed five times with H_2O, and then digested as described above. The method of removing dithionite–citrate–bicarbonate was tested by using artificial pure goethite powder (Bayferrox® 920Z, Lanxess) that was treated in triplicate by dithionite extraction and compared with results of the same goethite dissolved in HCl.

Iron isotope compositions were measured by MC-ICP-MS (Thermo-Finnigan Neptune instrument operated in high resolution and dynamic mode, University of Bonn, Germany; e.g., Weyer and Schwieters 2003). The sample solution was introduced into the plasma via a double pass Scott design quartz glass spray chamber. We used a Cu solution (Alfa Aesar, Specpure®) with $^{65}Cu/^{63}Cu=0.4457$ (calibrated against the IRMM-014 Fe reference material) for mass fractionation correction, thus following the approach outlined by Arnold et al. (2004) for Fe isotope analyses of soil samples. During every analytical session, Fe and Cu isotope ratios of a solution of the Fe standard IRMM-014 containing 2 μg mL^{-1} Cu exhibited an excellent correlation, thus permitting the use of Cu for an online mass fractionation correction (e.g., Schoenberg and von Blanckenburg 2005; Weyer et al. 2005). Every sample measurement was framed by analysis of the international Fe isotopic reference material IRMM-014 doped with Cu. The isotopic ratios of $^{56}Fe/^{54}Fe$ and $^{57}Fe/^{54}Fe$ are expressed by the delta notation in per mil (‰) units, e.g.,

$$\delta^{56}\mathrm{Fe} = [(R_{sa}/R_{std}) - 1] \cdot 1,000. \quad (2)$$

The expression R_{std} in Eq. 2 refers to the average of the standard ratios before and after sample analysis (e.g., Teutsch et al. 2009). An analogous equation was used for calculating $\delta^{57}Fe$. The method of combining the use of Cu and standard-sample bracketing to correct for mass fractionation and drift was tested via repeated analyses of whole-rock reference materials and a Fe salt in-house standard provided by the ETH Zürich, Switzerland.

3 Results

3.1 Soil properties

Figure 1 depicts a photograph of the soil profile and Table 2 summarizes the main soil properties. The parent material of the upper horizons is Holocene fluvial loam (0 to ~70 cm) that overlays Pleistocene glaciofluvial sand (starting at ~70 cm, 2Cr horizon). The main feature of the soil is the strong enrichment of Fe in the oximorphic Bg and CrBg horizons (up to 412 g kg^{-1} Fe) whereas in the oximorphic

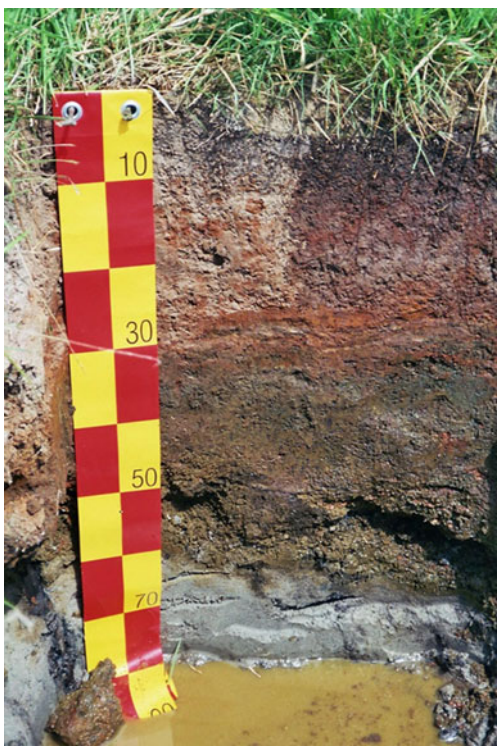

Fig. 1 Photograph of the Haplic Gleysol (Petrogleyic) developed from Holocene fluvial loam (0 to ~70 cm) that overlays Pleistocene glaciofluvial sand (starting at ~70 cm) at Lavesum in North Rhine-Westphalia, Germany (benchmark in 10-cm sections)

Ah horizon the Fe content is significantly lower. This massive enrichment of Fe is more or less cemented and popularly known as *bog iron* or *Raseneisenstein* and scholarly as petrogleyic (WRB and IUSS Working Group 2006). In the reductomorphic sandy 2Cr horizon, the Fe content is at a very low level (7.3 g kg^{-1} Fe). The slight increase of pH in the CrBg horizon coincides with the occurrence of inorganic C. All other horizons are free of inorganic C. According to the WRB and IUSS Working Group (2006), the soil is a Haplic Gleysol (Petrogleyic) due to the presence of a gleyic color pattern (Table 1).

3.2 Field dynamics of iron and other soil parameters

Table 2 shows results of the field monitoring program. Median depth to groundwater table was 27 cm during the course of the study. The groundwater level strongly varied between 83 cm below and 8 cm above soil surface. Maximum groundwater levels occurred during winter or after high precipitation events during the rest of the year. Soil horizons were water saturated for 126 (Ah), 328 (Bg), 437 (CrBg), and 840 days (2Cr) during the course of the investigation corresponding to 15% (Ah), 38% (Bg), 52% (CrBg), and 100% (2Cr at 120 cm depth), respectively. Soil temperatures were at about 11°C in median. Ranges declined with increasing soil depth. During the late spring, summer, and early autumn a capillary rise temporarily took place (as inferred from accompanying measurements of the soil matrix potential using tensiometers).

Reducing soil conditions were observed in all soil horizons following saturation with groundwater. Strongly reducing conditions (E_H<−100 mV) occurred in the 2Cr horizon (minimum, −179 mV, 120 cm) all over the time. In this permanently water-saturated horizon with its bluish gray color, Fe^{III} is thermodynamically not stable and oxidic Fe is virtually absent. Hence, this horizon was not considered for XRD, FTIR, and Mössbauer spectroscopy. Highest redox fluctuations occurred in the topsoil (range of 840 mV) and periodically strongly reducing conditions were obtained (minimum, −117 mV). The decrease of the E_H was both rapid and strong in this horizon. In both Fe-enriched horizons, the mean E_H was in a range indicating reduction of Fe^{III}. In agreement with the longer water saturation of the CrBg horizon (188 days compared to 142 days for the Bg horizon), both the median and the maximum E_H of the CrBg horizon were significantly lower in comparison to the Bg horizon. In this horizon, sometimes the E_H rose up to oxidizing conditions (+700 mV), which was never the case in the CrBg horizon.

In contrast to the pH of the bulk soil (pH 4.7 to 6.2, Table 2), the median pH of the soil solution (see Table 2) was around the neutral point due to H^+-consuming reducing processes at water saturation. Like in the soil extract, the pH in the soil solution was highest in the slightly calcareous CrBg horizon.

Iron concentrations in the shallow groundwater, represented by the soil solution obtained in the reductomorphic 2Cr, were at a high level of 44.8 mg L^{-1} (median, Table 2). It can be assumed that Fe under these pH/E_H conditions was nearly exclusively present as Fe^{2+}. Iron mobilization can be inferred from an increase in Fe concentrations of the soil solutions in the Ah (up to 8.6 mg L^{-1}), Bg (up to 5.9 mg L^{-1}), and CrBg (up to 4.3 mg L^{-1}) horizons, which occurred at reducing conditions. Since during reducing conditions no capillary rise occurred, we conclude that the increase in Fe concentrations resulted from the in situ reductive dissolution of Fe oxides.

3.3 Wet chemical iron oxide analyses

Oxalate-extractable Fe is the major Fe fraction in the Ah and the CrBg horizon with between 56% and 72% of oxidic Fe present in this fraction (see Table 2). In contrast, this fraction is only a minor one in the Bg horizon (23%). The difference between total Fe and dithionite-extractable Fe can be attributed to Fe bound in silicates and some organically complexed Fe. Unexpectedly, there seemed to

Table 1 Properties of the Haplic Gleysol (Petrogleyic) from Lavesum, Germany

Horizon	Depth (cm)	Soil texture	pH ($CaCl_2$)	OC (g kg^{-1})	IC (g kg^{-1})	N (g kg^{-1})	Fe[a] (g kg^{-1})	Fe_d[b] (g kg^{-1})	Fe_o[c] (g kg^{-1})	Fe_o/Fe_d	Mn (g kg^{-1})
Ah	0–15	Silty loam	4.7	73.9	n.d.	6.4	50	36	20	0.56	0.3
Bg	15–35	Silty loam	5.5	15.7	n.d.	1.0	316	275	62	0.23	1.5
CrBg	35–70	Loamy sand	6.2	22.3	1.8	0.7	412	390	280	0.72	1.5
2Cr	70–100+	Sand	4.7	1.7	n.d.	0.05	7.3	1.7	–[d]	–	0.07

OC organic carbon, *IC* inorganic carbon, *n.d.* not detectable

[a] Total iron

[b] Dithionite-extractable iron

[c] Oxalate-extractable iron

[d] Not determined

Table 2 Results of the field monitoring program

Parameter	Soil depth (cm)	Median	Minimum	Maximum
Depth to water table, cm	–	−27	−83	+8
Soil temperature, °C	10	11.0	2.4	22.1
	30	11.2	3.3	20.3
	50	11.3	4.3	18.8
	120	11.1	7.3	14.8
Redox potential, mV	10	506	−117	723
	30	190	−6	700
	50	8	−61	249
	120	−123	−179	−105
pH in soil solution	10	6.5	5.6	7.6
	30	7.2	6.9	7.5
	50	7.6	7.0	8.2
	120	6.9	6.4	7.8
Fe in soil solution, mg L^{-1}	10	1.6	0.2	8.6
	30	0.3	0.1	5.9
	50	0.6	0.2	4.3
	120	44.8	10.8	84.8
Dissolved organic carbon in soil solution, mg L^{-1}	10	41.3	17.9	52.0
	30	12.8	7.7	17.9
	50	4.2	1.9	8.3
	120	10.0	2.9	12.8

be great difference in the mineralogy of Fe between the Bg and the CrBg horizon as indicated by Fe_o/Fe_d.

3.4 X-ray diffraction analyses

Figure 2 displays the XRD patterns of random powder samples from the Ah, Bg, and CrBg horizon. In all horizons, quartz is the dominant mineral. Feldspars occur in minor amounts. Secondary chlorite (hydroxy-interlayered 2:1 layer silicate) is the only detectable clay mineral, with the highest amount occurring in the Ah horizon. In the CrBg horizon, only traces of secondary chlorite, visible as a shoulder in the XRD pattern near 7°2Θ, are present. Moderately acid soil conditions, as found in the Ah horizon, are optimal for formation of secondary chlorite. With increasing pH up to 6.2 in the CrBg horizon, the (Al, Fe) hydroxy interlayer becomes unstable and is nearly dissolved (Barnhisel and Bertsch 1989).

In the Ah horizon, no Fe oxides can be detected by XRD. In the Bg and CrBg horizon, goethite is the dominant mineral in addition to quartz. Moreover, siderite occurs in the CrBg horizon (Fig. 2 illustrates the four strongest siderite reflections).

The mean crystallite dimensions (MCD) of goethite in the Bg and CrBg horizon were calculated by the Scherrer

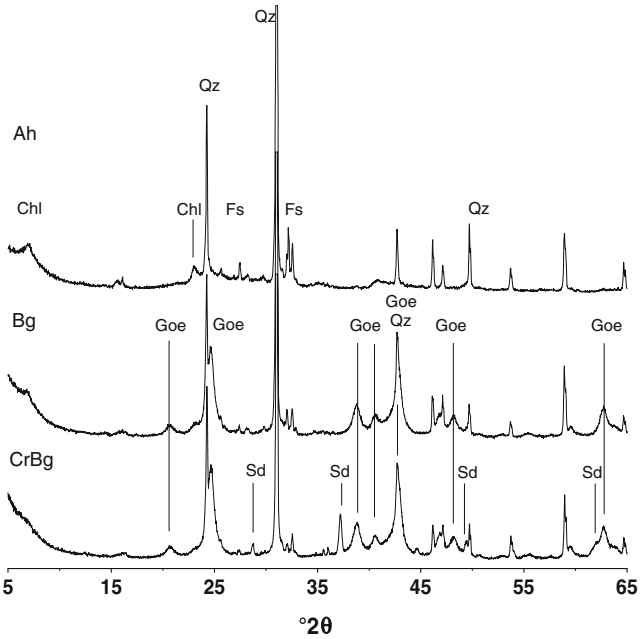

Fig. 2 Powder X-ray diffraction patterns (Co-Kα radiation) of random samples of the Ah, Bg, and CrBg horizon of the Haplic Gleysol (Petrogleyic). *Chl* secondary chlorite (hydroxy-interlayered mineral), *Qz* quartz, *Fs* feldspars, *Goe* goethite, *Sd* siderite

formula using the WHH (width at half height) of the four strongest goethite reflections. The calculation yields an average MCD of goethite of 20 nm with a standard deviation of 3 nm in the Bg as well as in the CrBg horizon. The corresponding WHH value of the 110 goethite line is 0.678°2Θ.

According to Schwertmann and Taylor (1989), variations of the particle size of goethite lead to a large range in the WHH of the XRD peaks, which may vary between 0.1 and 1.2°2Θ for the strongest (110) goethite line. Relatively sharp 110 peaks in the range of 0.3 to 0.7°2Θ are often observed in highly weathered tropical soils. In contrast, goethite that formed under reducing conditions in organic carbon-rich environments of temperate climates often has values in excess of 0.7°2Θ (Schwertmann and Taylor 1989).

3.5 Fourier transform infrared spectroscopy analyses

Fourier transform infrared spectroscopy analyses were performed as a complement to XRD analysis. The IR spectra confirm the presence of quartz in all samples. The characteristic band doublet of quartz (780 and 800 cm^{-1}) sometimes was masked by goethite bands but quartz could be identified by the sharp band at 690 cm^{-1}. The presence of feldspar is indicated by the band at 590 cm^{-1}, which was not detected in the Ah horizon, probably because of the lower feldspar content. However, the adjacent band at 600 cm^{-1} (goethite and/or apatite) is also supposed to affect

the 590 cm^{-1} signal. The spectrum of the samples from the CrBg and Bg horizons are dominated by goethite (3,140 cm^{-1}) and quartz (Fig. 3).

In addition, the presence of carbonates in the CrBg horizon was confirmed but could not be specified further due to their low intensity. The band position indicates the presence of either calcite or siderite but an unambiguous interpretation would only be possible by considering more bands which could not be resolved. By XRD and Mössbauer spectroscopy, siderite was identified, which explains the presence of the 1,420 cm^{-1} band. The Bg and Ah horizons only show a trace of carbonate (<<1 by mass%). This band (1,420 cm^{-1}) can also be explained by the presence of carboxylic groups of the organic matter.

The CrBg and Bg horizons show traces of kaolinite or halloysite less than <1 by mass% according to Madejova et al. (2002). The intensity of these bands appears to be slightly larger in the case of the Ah horizon and the larger kaolinite content of this sample is also indicated by the presence of the band at 915 cm^{-1} which is typical of dioctahedral clay minerals (AlAlOH). The low goethite content of the Ah horizon results in a well-resolved quartz doublet, in contrast to the other samples. XRD analysis of the Ah horizon showed the presence of a 14-Å mineral (chlorite, vermiculite, or smectite), which could not be detected by IR because of band coincidences with the dominating goethite.

Organic matter could be identified in all samples by the C–H stretching modes at 2,930 and 2,850 cm^{-1}. The Bg horizon contains less organic matter than the others (compare Table 2). The diffuse intensity around the water band at 1,630 cm^{-1} is attributed to functional groups of the organic matter.

Infrared spectroscopy can be used to further characterize Fe oxides. Houben and Kaufhold (2001, 2011) showed that the ratio of the band intensities at 3,430 to 3,140 cm^{-1} corresponds to the ferrihydrite/goethite ratio which in turn can be correlated with the N_2-BET specific surface area (pure ferrihydrite about 350 $m^2\ g^{-1}$, pure and well-crystallized goethite 20 $m^2\ g^{-1}$). The intensity ratio of the 3,430/3,140 cm^{-1} vibrations indicates the dominance of goethite over ferrihydrite in the CrBg horizon (IR band ratio 2.4) and indicates a slightly lower goethite/ferrihydrite ratio in the Bg horizon (IR band ratio 2.0).

3.6 Mössbauer spectroscopy

Figure 4 illustrates the Mössbauer spectra of the Ah, Bg, and CrBg horizons taken at 295 K (RT), 165 K, and 4.2 K. They show the presence of several Fe-containing phases in all horizons. Table 3 summarizes the quantitative assessment of these minerals.

The RT spectrum of the Ah horizon consists mainly of a doublet with a quadrupole splitting (QS) of 0.64 mm s^{-1}, an isomer shift (IS) of 0.26 mm s^{-1}, and a RA of 78%. This doublet represents Fe^{3+} that can be contained in a variety of phases, e.g., in nanocrystalline goethite, in ferrihydrite or in sheet silicates. A very weak (RA=2%) component of divalent Fe (QS=2.65 mm s^{-1}; IS=1.00 mm s^{-1}) is typical for Fe^{2+} in a sheet silicate. Well-crystallized goethite exhibits a magnetic sextet Mössbauer pattern at RT with a magnetic hyperfine field of about 37 T (Murad and Cashion 2004). Such pattern is not visible in the Mössbauer spectrum of the Ah horizon. Very small crystallites of goethite, however, are superparamagnetic at RT and then show only a quadrupole doublet with a splitting of about 0.52 mm s^{-1} (van der Zee et al. 2005). Cases in which goethite at RT exhibits a broadened magnetic pattern resulting from relaxation phenomena intermediate between the slow relaxation (sextet) and the fast relaxation (doublet) limit have also been observed (Ganguly et al. 1994; Govaert et al. 1976; Murad and Cashion 2004). The broad wings of the RT spectrum of the Ah horizon are typical for the latter type of goethite. Although they are expected to

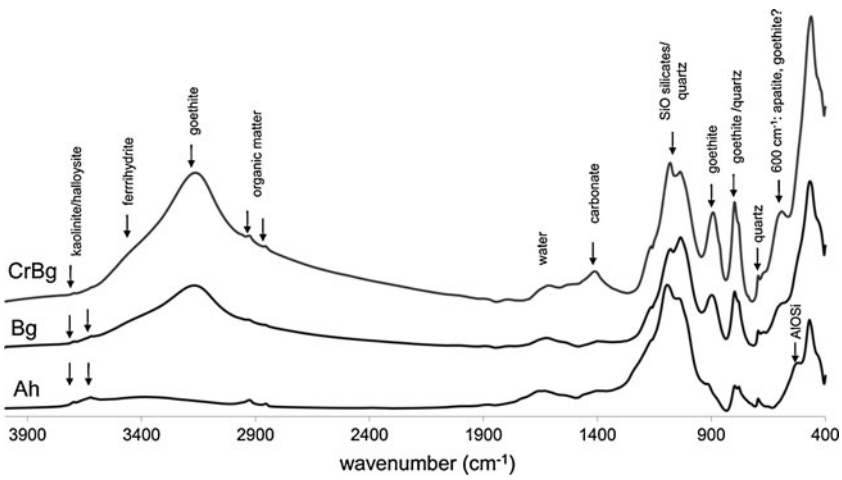

Fig. 3 Transmission FTIR spectra (KBr pellets) of the Ah, Bg, and CrBg horizon of the Haplic Gleysol (Petrogleyic) after drying at 150°C for 12 h

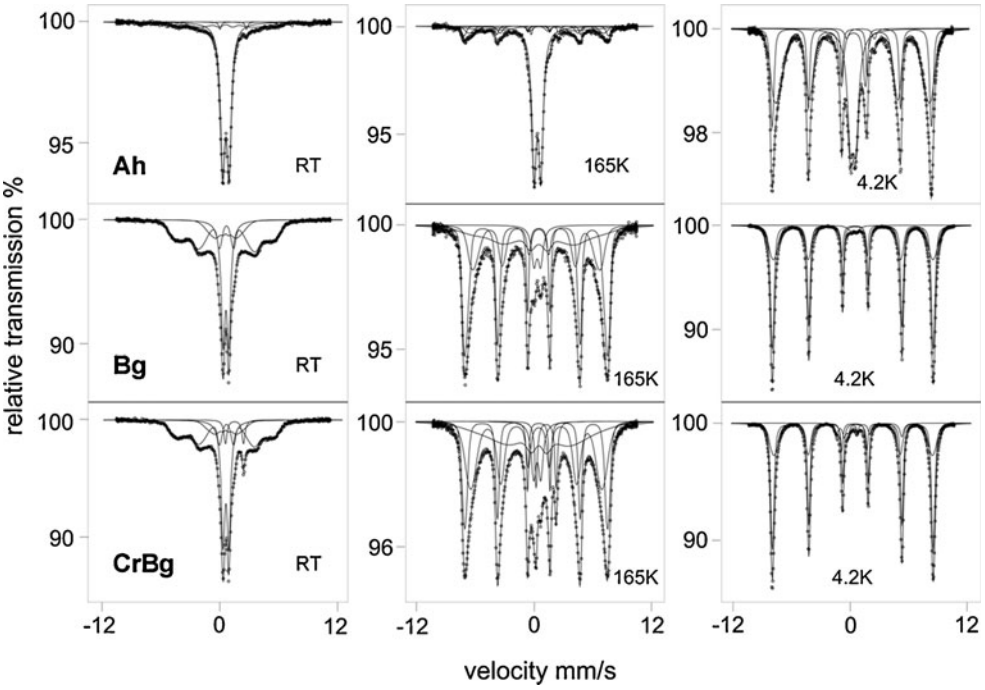

Fig. 4 Mössbauer spectra of the Ah, Bg, and CrBg horizon of the Haplic Gleysol (Petrogleyic) taken at room temperatures, 165 K and 4.2 K, with a source of ^{57}Co in rhodium having the same temperature as the absorber

represent a complicated relaxation pattern, for simplicity they were fitted assuming a Gaussian distribution of static magnetic hyperfine fields (mean field B_M=26 T; variance ΔB=9 T; RA=17%). There is also a weak indication (RA=3%) of a sextet pattern with a large hyperfine field of 52.2 T typical for hematite at RT.

The spectrum taken at 165 K allows a reliable distinction between goethite on the one hand and ferrihydrite and Fe in silicates on the other hand. Even nanocrystalline goethite that is superparamagnetic and hence showing only a doublet at RT is now expected to yield a magnetically split pattern, albeit with rather broad lines, while ferrihydrite still shows a superparamagnetic doublet at this temperature (Schwertmann et al. 2004). The magnetically split goethite component in the 165 K spectrum of the Ah horizon was fitted with a superposition of three sextets corresponding to Gaussian distributions of hyperfine fields. The total RA of the pattern attributable to goethite in the Ah horizon is 29%. The Fe^{3+} quadrupole doublet (QS=0.68 mm s^{-1}; IS=0.26 mm s^{-1}) has an area of 68% and may represent both ferrihydrite and Fe in a clay. The Fe^{2+} doublet (QS=2.75 mm s^{-1}; IS=1.00 mm s^{-1}; RA=2%) representing Fe in clay has the same intensity as at RT. The weak hematite component was fitted but is hardly visible in the spectrum.

The 4.2 K spectrum mainly consists of two magnetic components. One of these is attributable to goethite and could be fitted with a Lorentzian line sextet, a hyperfine field of B=49.7 T, QS=−0.54 and IS=0.25 mm s^{-1}, and RA=24%. The second component was fitted with an asymmetric Gaussian distribution of hyperfine fields, i.e., with a distribution that has a larger variance (ΔB_l) towards lower hyperfine fields than the most probable value and a smaller one (ΔB_h) towards higher fields, an approach that has been found to give good fits to the Mössbauer spectra of ferrihydrite (Eusterhues et al. 2008; Mikutta et al. 2008). The results (mean hyperfine field B_m=47.1 T; ΔB_l=3.5 T; ΔB_h=2.0 T; QS=−0.08 mm s^{-1}; IS=0.24 mm s^{-1}) are reasonable values for ferrihydrite, particularly when it is associated with soil organic matter (Eusterhues et al. 2008). The relative area of the ferrihydrite component is RA=51%. The Fe^{3+} quadrupole doublet still present at 4.2 K (QS=0.57 mm s^{-1}; IS=0.24 mm s^{-1}; RA=23%) as well as the weak Fe^{2+} doublet (IS=1.00 mm s^{-1}; QS=2.79 mm s^{-1}; RA=2%) are attributed to Fe in clay. Taking the 4.2 K results are the most reliable, one obtains the Fe contents in the different mineral phases given in Table 3.

The RT spectrum of the Bg horizon exhibits a quadrupole doublet and an additional broad magnetically split pattern.

Table 3 Presence of iron in the individual phases found by Mössbauer spectroscopy in three horizons of the Haplic Gleysol (Petrogleyic) from Lavesum, Germany

Horizon	Goethite, %	Ferrihydrite, %	Fe^{3+} (silicates), %	Fe^{2+} (silicates), %	Siderite, %
Ah	24	51	23	2	–
Bg	94	4	2	–	–
CrBg	86	7	–	–	7

Both can be attributed to nanocrystalline goethite with particles sizes either so small that the superparamagnetic relaxation is fast (doublet) or in the intermediate regime (broad sextet). This is similar to the Ah horizon, but the pattern representing particles showing intermediate relaxation is now much stronger, showing that there is now more goethite with larger particles. The mean particle size of 20 nm obtained from the XRD patterns fits well into this picture. The line shape of the magnetically split pattern was approximated by two static Gaussian distributions of hyperfine fields, one with a larger mean field (B_m=26.5 T; ΔB_l=10 T; ΔB_h=2.5 T; QS=−0.38 mm s^{-1}; IS=0.22 mm s^{-1}; RA=50%), and one with a rather small one (B_m=9.5 T; ΔB=2.0 T; RA=16%). The parameters of the quadrupole doublet attributed to rapidly relaxing superparamagnetic goethite are QS=0.57 and IS=0.26 mm s^{-1} and RA=34%.

Expectedly, at 165 K nearly all Fe is magnetically split with a rather broad pattern typical for small particle-size goethite at this temperature. This pattern was fitted like that of the Ah horizon, i.e., with a superposition of three symmetrical Gaussian distributions of hyperfine fields. The one with the largest hyperfine field is the narrowest one (B_m=44.4 T; ΔB=1.3 T; QS=−0.52 mm s^{-1}; IS=0.25(1) mm s^{-1}). There is, however, still a weak quadrupole doublet (QS=0.66 mm s^{-1}; IS=0.23 mm s^{-1}; RA=6%) that may be due to either ferrihydrite or Fe in clay. In any case, the spectrum shows that there is at best very little ferrihydrite in the Bg horizon.

In the 4.2 K spectrum of the Bg horizon there is still a very weak quadrupole doublet, but its intensity is now only RA=2%. This can be attributed to Fe in a minor clay phase. The remainder of the more intense doublet seen in the 165 K spectrum may be attributable to ferrihydrite that is magnetically split at 4.2 K but is no longer visible under the dominant magnetic sextet of goethite due to its low concentration. The goethite sextet is somewhat broadened and therefore was fitted by a superposition of a narrow Lorentzian sextet (B=49.8 T; QS=−0.55 mm s^{-1}; RA=61%) and a sextet resulting from a symmetric Gaussian distribution of hyperfine fields (B_m=49.4 T; ΔB=2.5 T; RA=37%). The distribution of the hyperfine fields of the goethite may be due to aluminum impurities or low crystallinity (Murad and Cashion 2004).

Assuming that, indeed, the broadened magnetic pattern observed at 4.2 K in the Bg horizon contains a minor ferrihydrite component, we conclude that 94% of the Fe is in goethite, 4% in ferrihydrite, and 2% in silicates. No Fe^{2+} is visible in the Bg horizon within the limits of experimental error.

The RT spectrum of the CrBg horizon is essentially like that of the Bg horizon and was fitted in the same manner, but there is an additional quadrupole doublet of Fe^{2+} with QS=1.77 and IS=1.16 mm s^{-1} and RA=7%. These parameters are practically those of siderite (Forester and Koon 1969; Srivastava 1985).

The 165 K spectrum is like that of the Bg horizon and was fitted in the same manner. It again contains a minor Fe^{3+} doublet (QS=0.72 mm s^{-1}; IS=0.23 mm s^{-1}; RA=7%) and the Fe^{2+} doublet attributable to siderite (QS=2.02 mm s^{-1}; IS=1.12 mm s^{-1}; RA=6%).

At 4.2 K, the spectrum of the CrBg horizon again is very much like that of horizon Bg. The dominant goethite component is virtually the same as in horizon Bg. The Fe^{3+} quadrupole doublet present at 165 K is no longer visible and the siderite doublet is also no longer present, since siderite orders magnetically at about 37 K (Frederichs et al. 2003). The magnetic pattern of siderite is only weakly visible in the spectrum, but its fitted hyperfine parameters (B=17.7 T; QS=2.00 mm s^{-1}; IS=1.15 mm s^{-1}) are in good agreement with literature values for siderite (Forester and Koon 1969; Srivastava 1985). The intensity (RA=8%) is in good agreement with those obtained at higher temperatures.

The CrBg horizon thus contains most of the Fe as goethite (86%), 7% of the Fe is in ferrihydrite according to the intensity of the quadrupole doublet at 165 K, and 7% of the Fe is bound in siderite.

3.7 Stable iron isotopes

Table 4 shows the results of the stable Fe isotope measurements of the four soil horizons and highlights the variability of Fe isotopic compositions in a groundwater-influenced soil. The results of the analyses of two reference materials (BIR-1 and an in-house Fe salt of the ETH Zürich) are in excellent agreement with data reported in earlier publications. Pure goethite (Bayferrox® 920Z) used to test the dithionite extraction method was, as expected, completely dissolved during Fe_d extraction. The δ^{57}Fe values of the Fe_d solutions overlap within analytical uncertainty the value of the same goethite dissolved in HCl (see Table 4). In addition, little variation was observed for all δ^{57}Fe values of the replicate Fe_d extracts, supporting the reliability of the extraction method, including the subsequent procedure of dithionite removal (Staubwasser et al. 2006). As expected from theoretical mass dependent fractionation, δ^{57}Fe is ~1.5 times higher than δ^{56}Fe.

The Ah horizon exhibits a relatively high δ^{57}Fe value of +0.29‰ when compared to the Bg and CrBg horizons with significantly lower δ^{57}Fe values of −0.30‰ and −0.19‰, respectively. The 2Cr horizon has a δ^{57}Fe value only slightly lower (+0.22‰) than that of the Ah horizon but contains much less total Fe (see Table 1). Both horizons were subject to completely different redox conditions (see section 3.2), differ extremely with respect of their abundance of C_{org} (see Table 1) and also most likely in their

Table 4 Iron isotope data of four soil horizons of the Haplic Gleysol (Petrogleyic) from Lavesum, Germany

Sample	δ^{56}Fe (‰)	2 s.d.	δ^{57}Fe (‰)	2 s.d.	n[a]
Ah	0.188	0.017	0.287	0.040	5
Bg	−0.215	0.037	−0.301	0.030	6
CrBg	−0.128	0.074	−0.188	0.051	6
2Cr	0.137	0.060	0.216	0.085	6
Fe_d Ah	0.142	0.027	0.194	0.071	3
Fe_d Ah[b]	0.141	0.031	0.202	0.029	3
res. Ah	0.301	0.040	0.429	0.061	3
res. Ah[b]	0.374	0.010	0.551	0.009	3
Fe_d 2Cr	0.039	0.032	0.058	0.070	3
Fe_d 2Cr[b]	0.035	0.012	0.065	0.076	3
res. 2Cr	0.234	0.027	0.316	0.008	2
res. 2Cr[b]	0.234	0.022	0.322	0.043	3
Fe_d Bayf.[c]	0.169	0.025	0.253	0.048	7
HCl Bayf.[d]	0.143	0.033	0.215	0.018	3
BIR-1[e]	0.049	0.032	0.071	0.054	4
	(0.050)	(0.039)	(0.102)	(0.015)	
	(0.060)	(0.041)	(0.09)	(0.013)	
Fe salt ETH[f]	−0.718	0.056	−1.056	0.055	8
	(−0.71)	(0.18)	(−1.05)	(0.12)	(98)
	(−0.73)	(0.10)	(−1.07)	(0.15)	(89)

Data included bulk soil samples, Fe_d extractions and their residues, reference materials, and test materials. For determination of the δ values, the IRMM-014 reference material was used

[a] Number of analyses

[b] Replicate digestion

[c] Mean results of three separate Fe_d extractions of artificial pure goethite (Bayferrox® 920Z, Lanxess)

[d] Digested in hot 7 M HCl

[e] Values in brackets given by Poitrasson et al. (2004) for δ^{57}Fe, Weyer et al. (2005) for δ^{56}Fe, and Williams et al. (2005) for δ^{57}Fe, respectively

[f] In-house salt standard of the ETH Zürich, Switzerland; values in brackets given by Teutsch et al. (2009) and Fehr et al. (2008), respectively

mineral compositions. However, their quite similar Fe isotope compositions suggest an involvement of different processes and/or mineral phases that ultimately resulted in the observed values (see below). In contrast, both the Bg and CrBg horizon are marked by a massive Fe enrichment (see Table 1) and the predominance of goethite (see Table 3), but significantly different δ^{57}Fe values. This may be attributed to preferential adsorption of heavy Fe isotopes during capillary rise of Fe-rich groundwater and/or partial dissolution of Fe oxides at reducing conditions (e.g., Beard et al. 2010; Brantley et al. 2001).

The variation of the δ^{57}Fe values with soil depth is illustrated in Fig. 5a. As is evident, there is no significant relationship between δ^{57}Fe and soil depth. To note, the isotope pattern of the Haplic Gleysol at Lavesum is somewhat similar to another Haplic Gleysol near Tettnang, Southern Germany, as reported by Wiederhold (2006; see Fig. 5b). In contrast, Fe concentrations are much higher and δ^{57}Fe values are significantly lower for the bulk Bg and CrBg horizons of the Gleysol at Lavesum. However, one concretion sampled at ~70 cm depth of the Gleysol at Tettnang by Wiederhold (2006) has a δ^{57}Fe value similar to the one of the massive goethite concretions in the CrBg horizon (Lavesum). Similar processes like precipitation and partial dissolution of Fe oxides formed the concretion in the Tettnang soil and the massive Fe enrichments in the Lavesum soil, and therefore resulted in similar Fe isotope compositions.

The Fe_d extracts and the residues after Fe_d extraction of the Ah and 2Cr horizon differ significantly (see Table 4). The Fe_d solutions of the two extractions from the Ah horizon are marked by δ^{57}Fe values of ~+0.20‰, whereas the remaining residues exhibit high δ^{57}Fe values of +0.43‰ and +0.55‰, respectively. The rather large variation of the δ^{57}Fe values of the two Ah residues is attributed to a heterogeneous silicate composition of this horizon. A low δ^{57}Fe value of ~+0.06‰ was observed for the Fe_d solutions from the 2Cr horizon, contrasting to again high δ^{57}Fe values of ~+0.32‰ for the residues which are similar to values reported for clastic sediments (Fantle and DePaolo 2004).

Recalculation of the bulk δ^{57}Fe value for the Ah horizon by using the Fe oxide—Fe silicate proportions given by the Mössbauer data (see Table 4) yields an average δ^{57}Fe of +0.27‰, which is within analytical uncertainty of the "true" value of +0.29‰. For the 2Cr horizon, no Mössbauer data exist. Instead, we used the Fe_d-Fe_{total} ratio calculated from data given in Table 2 as a proxy. This amounts to ~23% dithionite-extractable Fe and ~77% silicate-bound Fe. The calculated average δ^{57}Fe value of the 2Cr horizon is +0.26‰, again within analytical uncertainty of the measured value of +0.22‰. As a conclusion, recalculation of the bulk δ^{57}Fe values again demonstrated the robustness of analyzing Fe isotopes in Fe_d extracts and its residues.

4 Discussion

4.1 Field observations

The strong enrichment of Fe in the topsoil of soils influenced by high groundwater tables is a typical feature of Pleistocene sandy fluvial lowlands and has been observed in many corresponding landscapes of Central and Northern Europe, e.g., Belgium (Stoops 1983), Germany (Schlichting 1965), Denmark (Breuning-Madsen et al. 2000), and Poland (Kaczorek and Sommer 2003), but

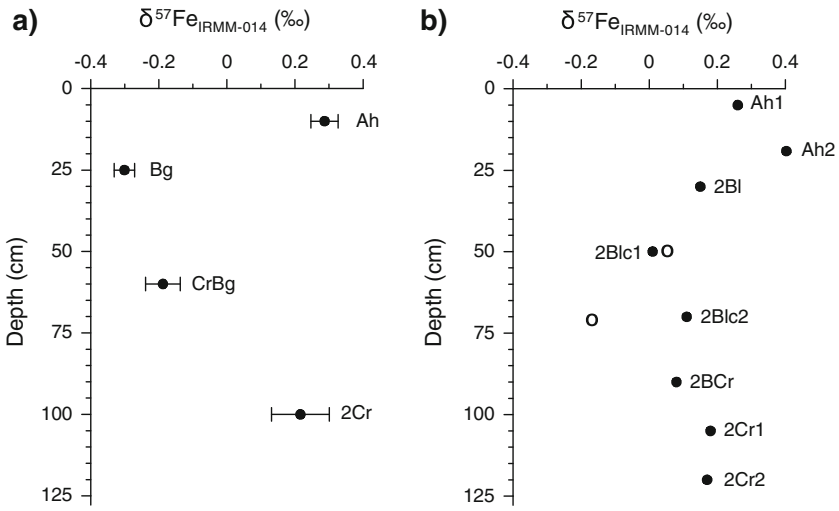

Fig. 5 Comparison of $\delta^{57}Fe_{IRMM-014}$ values of four horizons of the Haplic Gleysol (Petrogleyic; *left*, Fig. 5a; standard deviations are represented by *error bars*) with data of a Gleysol near Tettnang, Black Forest, southern Germany (*right*, Fig. 5b; Wiederhold 2006). The soil near Tettnang contains less Fe, but features local areas of Fe-rich redoximorphic zones. Their isotope compositions are shown as *open circles*

also in North America (Crerar et al. 1979). Petrogleyic horizons of such soils largely consist of Fe (~200 to ~500 g kg^{-1}) that is predominantly occurring as oxidic Fe, i.e., most of the total Fe can be extracted by Fe_d. This is also true for the Bg and CrBg horizons of our soil (see Table 1).

It is commonly accepted that the formation of petrogleyic properties is caused by the capillary rise of soil solutions that are enriched in Fe^{2+} (e.g., Blume 1988; Schlichting 1965). At a quasi-stationary O_2 barrier, Fe^{2+} is oxidized with the subsequent formation of Fe oxides. If the O_2 barrier (a) is near the surface and (b) fluctuates within a short distance (cm to few dm), and if (c) the soil solution contains sufficient Fe^{2+}, then (d) in the course of time Fe enrichment takes place. Higher concentrations of Fe in groundwater around areas with bog iron are caused by ligand-exchange induced dissolution of ferric compounds from podzolic soils, and/or reductive dissolution of Fe oxides under reducing conditions from gleyic soils. As pointed out by Banning et al. (2009), Fe in the groundwater of our catchment mainly originates from the weathering of Cenozoic paleo bog iron ores occurring in the Haltern layers (Santonian-Lower Campanian, Upper Cretaceous). They identified temporally and locally strongly reducing groundwater conditions within the Haltern layers by elevated dissolved Fe levels. Together with Fe, arsenic (As) is mobilized since the paleo bog iron contains significant amounts of this semimetal (mean, 43.9 mg kg^{-1} As; Banning et al. 2009). The groundwater moves through the Haltern layers towards Pleistocene glaciofluvial sands (thickness of 3 to 5 m; 2Cr horizon, see Fig. 1) and, by capillary rise, temporarily towards the overlaying Holocene fluvial loams (see Fig. 1). When coming into contact with O_2, Fe is rapidly immobilized by precipitation as Fe oxide. Arsenic, as well, precipitates together with Fe causing As contents of 626 mg kg^{-1} in the Bg, and 999 mg kg^{-1} As in the CrBg horizon, respectively (data not presented). We cannot exclude that some Fe originates from surrounding hills with thin podzolic soils. However, since these soils contain As at very low levels (about 1 mg kg^{-1}) we conclude that most of the petrogleyic Fe originally arises from the paleo bog iron.

From our field measurements, it is obvious that the above mentioned process of Fe enrichment in the Heubach plain is a recent one: (a) Fe is in excess in the near-surface groundwater (see Table 2), (b) a capillary rise temporarily took place, and (c) the Ah, Bg, and CrBg horizons are temporarily acting as a O_2 barrier as is evident from E_H measurements (see Table 2). Hence, the enrichment of Fe oxides at this site is not terminated but still in progress, and the Bg and CrBg horizons act as a sink for Fe. On the other hand, periods of reducing conditions occurred in all three horizons after water saturation. Critical redox potentials for the onset of soil Fe^{III} reduction are at 150 to 200 mV at pH 6 to 7 (Cogger et al. 1992; Mansfeldt 2004; Patrick and Jugsujinda 1992). Consequently, in these three horizons not only the precipitation and formation of Fe oxides occurred but also continuous dissolution and (re)-precipitation. Overall, a pronounced dynamic behavior of Fe is the main feature in these horizons. This should affect the mineralogy of Fe oxides and the isotopic composition of Fe.

4.2 Occurrence and properties of iron oxides and other iron phases

Studies dealing with the characterization of Fe oxides in soils with petrogleyic properties have mostly used either operationally defined selective chemical extractions and/or standard powder XRD techniques (see literature cited in 4.1). However, chemical extraction methods are not mineral selective. For example, acid-ammonium oxalate dissolves not only ferrihydrite but also for the most part, if not

completely nanogoethite (Thompson et al. 2006, 2011). Ferrihydrite is hardly to identify by XRD alone since it has broad and weak reflections, especially in complex mixtures like soils (Childs 1992), and crystalline Fe oxides can be identified in soils only at relatively high amounts (Cornell and Schwertmann 2003). All these shortcomings are reflected in our XRD and FTIR analyses since we did not detect any Fe oxides in the Ah horizon and no ferrihydrite in the Bg and CrBg horizon (see Fig. 2). In contrast, Mössbauer spectroscopy at cryogenic temperatures is well suited to identify and quantify the different pools of Fe phases in soils even at relatively low amounts (Rancourt 1998; van der Zee et al. 2003). Hence, this technique was chosen in order to clarify the solid phase speciation of Fe.

Iron phases identified by Mössbauer spectroscopy include ferrihydrite as well as goethite in all investigated horizons (see Fig. 4, Table 3). Additionally, siderite was detected in the CrBg horizon which was confirmed by XRD (see Fig. 2) and denoted by FTIR (see Fig. 3). Significant amounts of Fe occur as ferric Fe in silicates in the Ah horizon and smaller amounts in the Bg horizon. Ferrous Fe in silicates is only of minor importance (Ah horizon).

Ferrihydrite is intrinsically a short-range-ordered phase having very small particles of about 2 to 4 nm and a poor crystallinity. It is assumed that ferrihydrite is often the first phase to form in soils, especially at rapid oxidative precipitation (Cornell and Schwertmann 2003; Schneider 1988). As discussed above, the decrease of the E_H was both rapid and strong in the Ah horizon which can be explained by the high amounts of organic C (see Table 1) that acts as electron donor for microbial respiration. Additionally, the bioavailability of organic C in the topsoil should be high as a result of permanent inputs of fresh plant material, e.g., roots. The standard E_H and the rate of reductive dissolution of Fe oxides depend on type and crystallinity of the oxide, on mineral surface area, and on surface coverage (Fischer 1987; Jones et al. 2000; Ponnamperuma et al. 1967; Straub et al. 2001). As a result, ferrihydrite is the primary terminal electron acceptor for Fe-reducing bacteria rather than the crystalline forms (Roden and Zachara 1996; Zachara et al. 2002). Hence, we assume that in the Ah horizon ferrihydrite is preferentially dissolved by reductive dissolution after water saturation and at an adequate E_H (<150 mV, pH 7). Periods of reducing conditions were only temporary in the Ah horizon because O_2 rapidly entered the topsoil after falling water tables. Then, Fe^{2+} is rapidly oxidized and precipitated as ferrihydrite. However, under oxidizing conditions metastable ferrihydrite is gradually transformed to more thermodynamically stable and crystalline phases like goethite or hematite. This transformation depends, among other things, on the presence of solutes. It is well-known that natural organic matter effectively prevents the conversion of ferrihydrite to the more crystalline forms (Jones et al. 2009). Inherently, the Ah horizon contains the highest amount of organic matter as well as dissolved organic carbon of up to 52 mg C L^{-1} (see Table 1 and 2). The presence of such substances explains why the crystallization of goethite is prevented and why ferrihydrite is the dominating Fe mineral in the Ah horizon. The relatively low hyperfine field for the ferrihydrite in the 4.2 K Mössbauer spectrum supports the association of the ferrihydrite with organic matter. Overall, the Ah horizon exhibits the effects of short-term internal Fe cycling depending on the E_H. Nevertheless, we cannot exclude for the Ah horizon that some of the in situ produced Fe^{2+} was leached at periods of high precipitation (loss of Fe), and that some Fe^{2+} was introduced into the Ah horizon by capillary rise from the subsoil (gain of Fe).

Goethite is by far the dominating Fe phase both in the Bg and CrBg horizon. At first glance, this is a surprising finding as one might expect that repeated redox fluctuations promote the accumulation of ferrihydrite as it is the primary predicted mineral formed during rapid oxidative precipitation. What could be the reasons for the enrichment of goethite? One often mentioned aspect is that intermittent periods of anoxic conditions are thought to cause a depletion of ferrihydrite by reduction and removal of Fe^{2+} due to leaching, thus enriching the remaining soil in crystalline Fe oxides by simple mass balance (Cornell and Schwertmann 2003; Miller et al. 2001). This argument is unconvincing in the present case since the studied Gleysol all things considered is a strongly Fe enriching system due to the capillary rise of Fe^{2+}-containing soil solutions. Otherwise, petrogleyic properties could not have developed. Recently, Thompson et al. (2006) demonstrated in a laboratory study that redox fluctuations that span the Fe reduction/oxidation threshold promoted the direct conversion of short-range-ordered material into more crystalline forms (goethite and hematite) with no Fe removal from the soil. This secondary solid-state mineral transformation occurs under anaerobic conditions in the presence of Fe-reducing bacteria at relatively low Fe^{2+} concentrations (Hansel et al. 2003; Zachara et al. 2002), but also in pure Fe oxide systems to which Fe^{2+} was added (Jeon et al. 2003; Pedersen et al. 2005; Wei et al. 2011). The mineral transformation is explained by the catalytic action of the Fe^{2+} that is rapidly adsorbed to the surface of remaining ferrihydrite because electrons are transferred from adsorbed Fe^{2+} to structural Fe(III) (Williams and Scherer 2004). It is assumed that the ferrihydrite crystal lattice is broken up and more stable Fe phases like goethite are precipitated as new minerals (Manceau and Drits 1993; Pedersen et al. 2005). Both the Bg and the CrBg horizons contain Fe oxides in abundance, even at water saturation and under reducing conditions. Ferrous Fe that either enters these horizons by capillary rise or that is formed in situ by reductive

dissolution of Fe(III) might be adsorbed onto the surface of Fe oxides thus transforming short-range-ordered material (nanometer sized goethite) in the course of time into more crystalline phases. Hence, ferrihydrite is only a minor Fe phase in the Bg and CrBg horizons (4% and 7%, respectively). In contrast, goethite accumulates as a result of mineral transformation. The accumulation of goethite, once formed, is further promoted since, as outlined above, it is more resistant against microbial reductive dissolution than ferrihydrite. Van der Zee et al. (2003) postulated that diagenetic Fe cycling near the oxic–anoxic boundaries of lake and marine sediments occurs under conditions that directly lead to goethite precipitation, with growth poisoning from coprecipitation to produce nanoscale crystallites. They found nanogoethite with a mean size of only 5 nm, i.e., very similar to that of ferrihydrite. Whether this process plays also a role in terrestrial systems cannot be deduced from our approach.

Soil solution Fe^{2+} is not only removed by oxidation and adsorption but also by precipitation of sparingly soluble Fe^{II} minerals under reducing conditions. The formation of siderite ($FeCO_3$; Fredrickson et al. 1998; McMillan and Schwertmann 1998; Postma 1981), magnetite (Fe_3O_4; Lovley 1991), and vivianite ($Fe_3(PO_4)_2\ 8H_2O$; Fredrickson et al. 1998) are examples. Neither magnetite nor vivianite was detected in our samples, indicating that they are absent or present only in insignificant amounts below the detection limit. Siderite, however, was clearly identified in the CrBg horizon. The carbonate required for the siderite formation was not introduced via outside groundwaters as was the case in a Danish river bog (Postma 1981), because the groundwater of our catchment has pH values around 6. Instead, we assume that the carbonate was produced in situ by Fe^{III}-reducing bacteria, which generate both Fe^{II} and HCO_3^- with the latter being a product of the oxidation of organic matter (e.g., Konhauser 2007). Ferrous Fe and HCO_3^- then react according to Eq. 3

$$Fe^{2+}+HCO_3^-+OH^-\rightarrow FeCO_3+H_2O. \quad (3)$$

As pointed out by Zachara et al. (2002), siderite formation is encouraged by rapid reduction rates of ferrihydrite and concentrations of bicarbonate in the mmol L^{-1} range. It is unrealistic that such conditions exist in the CrBg horizon today. However, it should be taken into account that the enrichment of Fe at this site started in the Holocene (~5,000 years BP). Obviously, at that time or anytime thereafter, soil conditions were optimal for the formation of siderite. Remains of peat plants could sometimes be detected both in the Bg and CrBg horizon indicating that this site exhibited much higher water tables than today (drainage by ditches started not until in the late 19th century). Hence, we assume that conditions for siderite formation were formerly also favorable in the Bg horizon. In contrast to the CrBg horizon, however, siderite is not present in the Bg horizon today. This finding is in agreement with the observation that the Bg horizon was frequently in contact with O_2. We suppose that under oxidizing conditions siderite weathers by oxidation to goethite as stated by McMillan and Schwertmann (1998). This transformation is another option for the formation and enrichment of goethite in this soil.

We have repeatedly pointed out that the extraction with oxalate is not specifically selective for ferrihydrite. Reasons for this include (see Cornell and Schwertmann 2003): (a) Fe associated with organic matter will also be extracted by oxalate; however, in mineral soil horizons as in our case this fraction is only of minor importance; (b) oxalate dissolves goethite with very small particle size, i.e., nanogoethite; both in the Bg and CrBg horizon such goethite is present, presumably occurring in a rather broad continuum of size and crystallinity; and (c) if large amounts of Fe(II) compounds are present in a sample, the released Fe^{2+} will catalyze the dissolution of more crystalline Fe oxides in an oxalate solution; obviously, this interference plays an important role in the CrBg horizon since it contains significant amounts of siderite. In summary, values of Fe_o/Fe_d are difficult to interpret in the Bg and CrBg horizons.

4.3 Stable iron isotopes

The Haplic Gleysol near Lavesum is characterized by a relatively broad range of $\delta^{57}Fe$ values ($\Delta^{57}Fe_{Ah-Bg}=\delta^{57}Fe_{Ah}-\delta^{57}Fe_{Bg}=0.59‰$) and a massive Fe enrichment within a depth range of a few dm. At a first glance, there seems to be little difference between the upper- and the lowermost horizon (Ah and 2Cr, respectively) with regard of the Fe isotope composition, because the $\delta^{57}Fe$ values are quite similar (+0.29‰ and +0.22‰). Field observations, Fe abundance, and mineral composition, however, clearly show that these two horizons have otherwise little in common. In strong contrast, the Bg and CrBg horizons have the highest and quite similar abundances of goethite (see Table 3) and total Fe (see Table 1), but a larger $\Delta^{57}Fe$ of −0.11‰ (= $\delta^{57}Fe_{Bg}-\delta^{57}Fe_{CrBg}$) than Ah vs. 2Cr horizon. A similar observation, although less pronounced, was made by Wiederhold (2006) for a Gleysol less enriched in Fe but still with local Fe concretions (see Fig. 5b). What are possible processes and causes that result in the observed Fe isotope variations in the soil profile?

As noted in the section 1, earlier studies have shown that fractionation of Fe isotopes in soils can be mediated by abiotic processes (proton-promoted or ligand-controlled Fe oxide dissolution, adsorption of Fe onto existing Fe oxides, mineral transformation), biotic processes (microbial Fe^{III} reduction or Fe^{II} oxidization), and a combination of both

pathways. The Fe isotope composition of a soil horizon is therefore a result of a complex interaction of processes.

Weathering of rocks is one of the fundamental factors of pedogenesis. The slow process of silicate weathering results in a net loss of ^{54}Fe and a heavy Fe isotope signature in the residual silicate phases (Fantle and DePaolo 2004; Guelke et al. 2010; Kiczka et al. 2010; Thompson et al. 2007; Wiederhold et al. 2007b). The Ah and the 2Cr horizon contain both silicate-bound Fe, but in different proportions as shown by Mössbauer data and Fe_d extraction, respectively. For the Fe-poor glaciofluvial sand of the 2Cr horizon, silicate-bound Fe obviously controls the isotope composition that is close to values reported by Fantle and DePaolo (2004) for other clastic sediments. The Fe isotope composition of the Ah horizon on the other hand is largely dominated by Fe oxides. However, the δ^{57}Fe values of the clay minerals present in the Ah (i.e., the residue after Fe_d extraction) are high which is in accord for the observed effect of weathering on the Fe isotope composition of rocks and minerals.

Faster processes related to Fe isotope fractionation are dissolution and (re-)precipitation of Fe oxides with the heavy Fe isotopes precipitating preferentially (Bullen et al. 2001; Jang et al. 2008). As observed in the field, Fe enrichment of groundwater in the area (see Table 3) results from slow weathering of bog iron in the Haltern layers (Banning et al. 2009). The dissolved Fe will carry a comparatively light Fe isotope signature because only thin layers of the bog iron are dissolved and ^{54}Fe enters the solution predominantly during breakdown of Fe oxides (Brantley et al. 2004; Johnson et al. 2004). As an example, low δ^{57}Fe values of −0.57‰ were observed by Teutsch et al. (2005) in groundwater of a floodplain in central Switzerland. If nanogoethite precipitates from Fe-rich water along an oxic–anoxic boundary as suggested by van der Zee et al. (2003), its Fe isotope composition would be slightly heavier compared to the groundwater (depending on the amount of oxidized Fe), unless all Fe is removed from the water and oxidized to goethite. Obviously, precipitation of Fe oxides is not occurring quantitatively in a small area, but gradually over a long distance (e.g., Kaczorek and Sommer 2003), which in turn is expected to result in a gradual depletion of heavy Fe isotopes in the groundwater (e.g., Mikutta et al. 2009). Siderite is only a minor Fe phase with respect to goethite in the CrBg horizon, however it still may contribute to the overall light Fe isotope signature because it seems to incorporate ^{54}Fe preferentially during precipitation as suggested by Wiesli et al. (2004) in an experimental study and observed by Markl et al. (2006) in nature. Moreover, Markl et al. (2006) showed that Fe isotope fractionation during slow transformation at low temperatures of siderite to goethite via oxidation is negligible, i.e., the present-day goethite could have partially inherited a former siderite Fe isotope signature (see section 4.2).

If Fe oxides like goethite are present in a soil horizon, the heavy isotopes of the Fe species in solution will be preferentially adsorbed onto existing goethite during a capillary rise of Fe-rich water (see e.g., Beard et al. 2010; Brantley et al. 2004; Icopini et al. 2004; Jang et al. 2008; Mikutta et al. 2009). The Bg and CrBg horizon are marked by the lowest δ^{57}Fe values and highest goethite abundances in our soil profile, seemingly in contrast with preferential adsorption of heavy Fe isotopes. However, as mentioned above, the groundwater is gradually depleted of Fe by oxidative precipitation and adsorption, thus resulting in low δ^{57}Fe values and lowest Fe concentrations in the groundwater (see Table 2). The effect of adsorption was demonstrated by Teutsch et al. (2005) in an experimental approach by introduction of O_2-rich water into a Fe-rich aquifer. Consequently, this triggered preferential adsorption of dissolved heavy Fe onto existing goethite, and shifted the δ^{57}Fe value of the water to extremely low values of ~−4‰. In conclusion, adsorption of heavy Fe isotopes occurring in the goethite-rich CrBg horizon during a rise of groundwater entails a comparatively lower δ^{57}Fe value of the overlying Bg horizon.

Organic matter and microbial activity are largely restricted to the topsoil (the Ah horizon in our study, see Table 1) and may affect fractionation of Fe isotopes as well. During the course of 28 months, the Ah horizon was subject to reducing conditions only ~15% of the time. Iron mobilization via Fe reduction is therefore largely limited to high groundwater levels. In this case, however, both relative fast aeration due to high activity of atmospheric O_2 and the presence of dissolved organic matter resulted in a predominant formation of short-range ordered ferrihydrite and ligand-complexed Fe. In a soil, a falling water table induces oxidation of free Fe^{2+} in solution as a fast process and decay of organic matter carrying Fe^{2+} as a slow process. Consequently, the heavy Fe isotopes are removed from solution preferentially during precipitation, thus forming relatively heavy ferrihydrite and/or nanogoethite. Moreover, other authors (e.g., Beard et al. 1999; Brantley et al. 2001, 2004; Crosby et al. 2005; Wiederhold et al. 2007a) argue that microbial reduction of Fe may result in high δ^{57}Fe values in Fe depleted soil horizons (i.e., the Ah horizon in our study). Obviously, microbial activity is highest in the Ah horizon, thus it needs to be taken into account for fractionation of Fe isotopes. Ultimately, both processes (oxidative precipitation, microbial activity) yield topsoil enriched in the heavy Fe isotopes and thus higher δ^{57}Fe values.

5 Conclusions

Our results indicate that under prolonged water saturation and prevailing reducing conditions, goethite rather than

ferrihydrite is the predominant Fe oxide in subsoil enriched with Fe. Goethite preferentially occurs as small particles, i. e., as nanogoethite. If Fe^{2+} accelerates the transformation of ferrihydrite to the more crystalline Fe oxides, then the Fe (III) pool in soils with reducing conditions is rather dynamic and not static. Compared to ferrihydrite, the crystalline Fe(III) species differs in two important environmental aspects: On the one hand, their surface areas are (much) lower, thus decreasing their sorption capacity for nutrients like phosphate or pollutants like arsenate; on the other hand, however, this pool is less reactive for microbial reduction, thus stabilizing them as an adsorber. Overall, this underlines the importance of the knowledge about the formation of Fe oxides as well as their precise identification in such soils. The latter is not achieved by traditional selective chemical extractions. Iron isotope data elucidated the cycle of Fe in groundwater-influenced soils und support the concept of a rather dynamic Fe pool. Although the Ah and the 2Cr horizons exhibit relatively similar high δ^{57}Fe values, fast ferrihydrite precipitation during high water tables and microbial activity promote a heavy isotope signature in the upper soil, whereas the permanently water-saturated Fe-poor horizon mostly shows the Fe isotope signature of silicates. The low δ^{57}Fe values in the extremely Fe-rich horizons (Bg, CrBg) are possibly the result of goethite formation in Fe-rich groundwater with a light Fe isotope composition and/or transformation of an isotopically light ferrihydrite or siderite precursor. Preferential adsorption of heavy Fe isotopes during capillary rise of Fe-rich groundwater through goethite-rich layers both lowers the Fe content of the water and gradually shifts its isotope composition to low δ^{57}Fe values. Iron oxides above such a goethite-rich layer are then marked by a comparatively low δ^{57}Fe value.

Acknowledgments For the assistance in the field and laboratory, we are grateful to Karin Greef, Julia Hurraß, Katrin Matern, Kristof Dorau, and Nadine Gorican. Ambre Luguet, University of Bonn, kindly helped to keep the Neptune operational. Jan Wiederhold from ETH Zürich is thanked for the Fe salt in-house isotope standard, Carsten Münker from the University of Köln for the BIR-1 reference material, and Hendrik Kathrein from Lanxess, Germany, for the Bayferrox 920Z goethite. This study was funded by the DFG (German Research Foundation) under the contract number Ma 2143/8-1 granted to T. Mansfeldt.

References

Arnold GL, Weyer S, Anbar AD (2004) Fe isotope variations in natural materials measured using high mass resolution multiple collector ICPMS. Anal Chem 76:322–327

Banning A, Coldewey WG, Gobel P (2009) A procedure to identify natural arsenic sources, applied in an affected area in North Rhine-Westphalia, Germany. Environ Geol 57:775–787

Barnhisel RI, Bertsch PM (1989) Chlorites and hydroxy-Interlayered vermiculite and smectite. In: Dixon JB, Weed SB (ed) Minerals in soil environments. Book series No.1, 2nd edn. Soil Sci Soc Am, Madison, USA, pp 729–788

Beard BL, Johnson CM (2004) Fe isotope variations in the modern and ancient earth and other planetary bodies. In: Johnson CM, Beard BL, Albarede F (eds) Geochemistry of non-traditional stable isotopes. Reviews in Mineralogy & Geochemistry. Mineralogical Society of America, Washington, pp 319–357

Beard BL, Johnson CM, Cox L, Sun H, Nealson KH, Aguilar C (1999) Iron isotope biosignatures. Science 285:1889–1892

Beard BL, Handler RM, Scherer MM, Wu L, Czaja AD, Heimann A, Johnson CM (2010) Iron isotope fractionation between aqueous ferrous iron and goethite. Earth Planet Sci Lett 295:241–250

Bigeleisen J (1965) Chemistry of isotopes. Science 147:463–471

Blume HP (1988) The fate of iron during soil formation in humid-temperate environments. In: Stucki JW (ed) Iron in soils and clay minerals. Reidel, Dordrecht, pp 749–777

Blume HP, Schwertmann U (1969) Genetic evaluation of profile distribution of aluminum, iron, and manganese oxides. Soil Sci Soc Am Proc 33:438–444

Bowell RJ (1994) Sorption of arsenic by iron oxides and oxyhydroxides in soils. Appl Geochem 9:279–286

Brantley SL, Liermann L, Bullen TD (2001) Fractionation of Fe isotopes by soil microbes and organic acids. Geology 29:535–538

Brantley SL, Liermann LJ, Guynn RL, Anbar A, Icopini GA, Barling J (2004) Fe isotopic fractionation during mineral dissolution with and without bacteria. Geochim Cosmochim Acta 68:3189–3204

Breuning-Madsen H, Ronsbo J, Holst MK (2000) Comparison of the composition of iron pans in Danish burial mounds with bog iron and spodic material. Catena 39:1–9

Bullen TD, White A, Childs CW, Vivit DV, Schulz MS (2001) Demonstration of significant abiotic iron isotope fractionation in nature. Geology 29:699–702

Childs CW (1992) Ferrihydrite: a review of structure, properties and occurrence in relation to soils. Z Pflanzenernähr Bodenk 155:441–448

Clayton RE, Hudson-Edwards KA, Malinovsky D, Andersson P (2005) Fe isotope fractionation during the precipitation of ferrihydrite and transformation of ferrihydrite to goethite. Mineral Mag 69:667–676

Cogger CG, Kennedy PE, Carlson D (1992) Seasonally saturated soils in the Puget Lowland II. Measuring and interpreting redox potentials. Soil Sci 154:50–58

Cornell RM, Schwertmann U (2003) The iron oxides. Structure, properties, reactions, occurrences and uses, 2nd edn. Wiley-VHC, Weinheim

Cornu S, Cattle JA, Samouelian A, Laveuf C, Guilherme LRG, Alberic P (2009) Impact of redox cycles on manganese, iron, cobalt, and lead in nodules. Soil Sci Soc Am J 73:1231–1241

Crerar DA, Knox GW, Means JL (1979) Biogeochemistry of bog iron in the New Jersey Pine Barrens. Chem Geol 24:111–135

Croal LR, Johnson CM, Beard BL, Newman DK (2004) Iron isotope fractionation by Fe(II)-oxidizing photoautotrophic bacteria. Geochim Cosmochim Acta 68:1227–1242

Crosby HA, Johnson CM, Roden EE, Beard BL (2005) Coupled Fe (II)-Fe(III) electron and atom exchange as a mechanism for Fe isotope fractionation during dissimilatory iron oxide reduction. Environ Sci Technol 39:6698–6704

Eusterhues K, Wagner FE, Hausler W, Hanzlik M, Knicker H, Totsche KU, Kogel-Knabner I, Schwertmann U (2008) Characterization of ferrihydrite-soil organic matter coprecipitates by X-ray diffraction and Mossbauer spectroscopy. Environ Sci Technol 42:7891–7897

Eusterhues K, Rennert T, Knicker H, Kogel-Knabner I, Totsche KU, Schwertmann U (2011) Fractionation of organic matter due to reaction with ferrihydrite: coprecipitation versus adsorption. Environ Sci Technol 45:527–533

Fantle MS, DePaolo DJ (2004) Iron isotopic fractionation during continental weathering. Earth Planet Sci Lett 228:547–562
Fehr MA, Andersson PS, Halenius U, Morth CM (2008) Iron isotope variations in Holocene sediments of the Gotland Deep, Baltic Sea. Geochim Cosmochim Acta 72:807–826
Fiedler S, Vepraskas MJ, Richardson JL (2007) Soil redox potential: Importance, field measurements, and observations. Adv Agron 94:1–54
Fischer WR (1987) Standard potentials (Eh°) of iron(III) oxides under reducing conditions. Z Pflanzenernähr Bodenk 150:286–289
Forester DW, Koon NC (1969) Mössbauer investigation of metamagnetic $FeCO_3$. J Appl Phys 40:1316–1317
Frederichs T, von Dobeneck T, Bleil U, Dekkers MJ (2003) Towards the identification of siderite, rhodochrosite, and vivianite in sediments by their low-temperature magnetic properties. Phys Chem Earth 28:669–679
Fredrickson JK, Zachara JM, Kennedy DW, Dong HL, Onstott TC, Hinman NW, Li SM (1998) Biogenic iron mineralization accompanying the dissimilatory reduction of hydrous ferric oxide by a groundwater bacterium. Geochim Cosmochim Acta 62:3239–3257
Ganguly B, Huggins FE, Feng Z, Huffman GP (1994) Anomalous recoilless fraction of 30-Å-diameter FeOOH particles. Phys Rev B 49:3036–3042
Golden DC, Turner FT, SittertzBhatkar H, Dixon JB (1997) Seasonally precipitated iron oxides in a vertisol of southeast Texas. Soil Sci Soc Am J 61:958–964
Govaert A, Dauwe C, Plinke P, De Grave E, De Sitter J (1976) A classfication of goethite minerals based on the Mössbauer behaviour. J Phys Coll 37:825–827
Guelke M, von Blanckenburg F, Schoenberg R, Staubwasser M, Stuetzel H (2010) Determining the stable Fe isotope signature of plant-available iron in soils. Chem Geol 277:269–280
Hansel CM, Benner SG, Neiss J, Dohnalkova A, Kukkadapu RK, Fendorf S (2003) Secondary mineralization pathways induced by dissimilatory iron reduction of ferrihydrite under advective flow. Geochim Cosmochim Acta 67:2977–2992
Herbel M, Fendorf S (2006) Biogeochemical processes controlling the speciation and transport of arsenic within iron coated sands. Chem Geol 228:16–32
Houben G, Kaufhold S (2001) Estimating the surface area of iron oxihydroxides from infrared (IR) spectrometry data. Supplements Eur J Min 13:86, Schweizerbart'sche Verlagsbuchhandlung, Stuttgart
Houben G, Kaufhold S (2011) Multi-method characterization of the ferrihydrite to goethite transformation. Clay Miner 46 (in press)
Icopini GA, Anbar AD, Ruebush SS, Tien M, Brantley SL (2004) Iron isotope fractionation during microbial reduction of iron: The importance of adsorption. Geology 32:205–208
Jang JH, Mathur R, Liermann LJ, Ruebush S, Brantley SL (2008) An iron isotope signature related to electron transfer between aqueous ferrous iron and goethite. Chem Geol 250:40–48
Jeon BH, Dempsey BA, Burgos WD (2003) Kinetics and mechanisms for reactions of Fe(II) with iron(III) oxides. Environ Sci Technol 37:3309–3315
Johnson CM, Beard BL, Roden EE, Newman DK, Nealson KH (2004) Isotopic constraints on biogeochemical cycling of Fe. In: Johnson CM, Beard BL, Albarede F (eds), Geochemistry of non-traditional stable isotopes. Reviews in Mineralogy & Geochemistry. Mineralogical Soc America, Washington, pp 359–408
Jones CA, Langner HW, Anderson K, McDermott TR, Inskeep WP (2000) Rates of microbially mediated arsenate reduction and solubilization. Soil Sci Soc Am J 64:600–608
Jones AM, Collins RN, Rose J, Waite TD (2009) The effect of silica and natural organic matter on the Fe(II)-catalysed transformation and reactivity of Fe(III) minerals. Geochim Cosmochim Acta 73:4409–4422
Kaczorek D, Sommer M (2003) Micromorphology, chemistry, and mineralogy of bog iron ores from Poland. Catena 54:393–402
Kappler A, Johnson CM, Crosby HA, Beard BL, Newman DK (2010) Evidence for equilibrium iron isotope fractionation by nitrate-reducing iron(II)-oxidizing bacteria. Geochim Cosmochim Acta 74:2826–2842
Kiczka M, Wiederhold JG, Frommer J, Kraemer S, Bourdon B, Kretzschmar R (2010) Iron isotope fractionation during proton- and ligand-promoted dissolution of primary phyllosilicates. Geochim Cosmochim Acta 74:3112–3128
Kiem R, Kögel-Knabner I (2002) Characterization of refractory organic carbon in particle-size fractions of arable soils: II. Organic carbon in relation to mineral surface area and iron oxides in fraction <6 μm. Org Geochem 33:1699–1713
Konhauser K (2007) Introduction to Geomicrobiology. Blackwell, London
Lovley DR (1991) Magnetite formation during microbial dissimilatory iron reduction. In: Frankel RB, Blakemore RP (eds) Iron biominerals. Plenum Press, New York, pp 151–166
Madejova J, Keckes J, Paalkova H, Komadel P (2002) Identification of components in smectite/kaolinite mixtures. Clay Min 37:377–388
Manceau A, Drits VA (1993) Local structure of ferrihydrite and feroxyhite by EXAFS spectroscopy. Clay Min 28:165–184
Mansfeldt T (2003) In situ long-term redox potential measurements in a dyked marsh soil. J Plant Nutr Soil Sci 166:210–219
Mansfeldt T (2004) Redox potential of bulk soil and soil solution concentration of nitrate, manganese, iron, and sulfate in two Gleysols. J Plant Nutr Soil Sci 167:7–16
Markl G, von Blanckenburg F, Wagner T (2006) Iron isotope fractionation during hydrothermal ore deposition and alteration. Geochim Cosmochim Acta 70:3011–3030
McMillan SG, Schwertmann U (1998) Morphological and genetic relations between siderite, calcite and goethite in a Low Moor Peat from southern Germany. Eur J Soil Sci 49:283–293
Mehra OP, Jackson ML (1960) Iron oxide removal from soils and clays by a dithionite-citrate system buffered with sodium bicarbonate. Clays Clay Min 7:317–327
Mikutta C, Mikutta R, Bonneville S, Wagner F, Voegelin A, Christl I, Kretzschmar R (2008) Synthetic coprecipitates of exopolysaccharides and ferrihydrite. Part I: characterization. Geochim Cosmochim Acta 72:1111–1127
Mikutta C, Wiederhold JG, Cirpka OA, Hofstetter TB, Bourdon B, Von Gunten U (2009) Iron isotope fractionation and atom exchange during sorption of ferrous iron to mineral surfaces. Geochim Cosmochim Acta 73:1795–1812
Miller AJ, Schuur EAG, Chadwick OA (2001) Redox control of phosphorus pools in Hawaiian montane forest soils. Geoderma 102:219–237
Murad E, Cashion J (2004) Mössbauer spectroscopy of environmental materials and their industrial utilization. Kluwer Academic Publishers, Dordrecht
Patrick WH, Jugsujinda A (1992) Sequential reduction and oxidation of inorganic nitrogen, manganese, and iron in flooded soil. Soil Sci Soc Am J 56:1071–1073
Patrick WH, Khalid RA (1974) Phosphate release and sorption by soils and sediments—effect of aerobic and anaerobic conditions. Science 186:53–55
Pedersen HD, Postma D, Jakobsen R, Larsen O (2005) Fast transformation of iron oxyhydroxides by the catalytic action of aqueous Fe(II). Geochim Cosmochim Acta 69:3967–3977
Peretyazhko T, Sposito G (2005) Iron(III) reduction and phosphorous solubilization in humid tropical forest soils. Geochim Cosmochim Acta 69:3643–3652
Poitrasson F, Halliday AN, Lee DC, Levasseur S, Teutsch N (2004) Iron isotope differences between Earth, Moon, Mars and Vesta as possible records of contrasted accretion mechanisms. Earth Planet Sci Lett 223:253–266

Ponnamperuma FN, Tianco EM, Loy T (1967) Redox equilibria in flooded soils: I. The iron hydroxide systems. Soil Sci 103:371–382
Postma D (1981) Formation of siderite and vivianite and the pore-water composition of a recent bog sediment in Denmark. Chem Geol 31:225–244
Rancourt DG (1998) Mössbauer spectroscopy in clay science. Hyperfine Interact 117:3–38
Roden EE, Zachara JM (1996) Microbial reduction of crystalline iron (III) oxides: Influence of oxide surface area and potential for cell growth. Environ Sci Technol 30:1618–1628
Sah RN, Mikkelsen DS, Hafez AA (1989) Phosphorus behavior in flooded-drained soils.2. Iron transformation and phosphorus sorption. Soil Sci Soc Am J 53:1723–1729
Schauble EA, Rossman GR, Taylor HP (2001) Theoretical estimates of equilibrium Fe-isotope fractionations from vibrational spectroscopy. Geochim Cosmochim Acta 65:2487–2497
Schlichting E (1965) Die Raseneisenbildung in der nordwestdeutschen Podsol-Gley-Landschaft. Chemie der Erde 24:11–26
Schneider W (1988) Iron hydrolysis and the biochemistry of iron—the interplay of hydroxide and biogenic ligands. Chimia 42:9–20
Schoenberg R, von Blanckenburg F (2005) An assessment of the accuracy of stable Fe isotope ratio measurements on samples with organic and inorganic matrices by high-resolution multi-collector ICP-MS. Int J Mass Spectrom 242:257–272
Schwertmann U (1964) Differenzierung der Eisenoxide des Bodens durch Extraktion mit Ammoniumoxalat-Lösung. Z Pflanzenernähr Düng Bodenk 105:194–202
Schwertmann U, Taylor RM (1989) Iron oxides. In: Dixon JB, Weed SB (eds) Minerals in soil environments. Book series No.1, 2nd edn. Soil Sci Soc Am, Madison, USA, pp 379–438
Schwertmann U, Friedl J, Kyek A (2004) Formation and characterization of a continuous crystallinity series of synthetic ferrihydrites and their relation to FeOOH forms. Clays Clay Min 52:221–226
Shaw JN, Odom JW, Hajek BF (2003) Soils on quaternary terraces of the Tallapoosa River, central Alabama. Soil Sci 168:707–717
Srivastava KKP (1985) Effect of orbit-lattice interaction in Mössbauer studies: quadrupole splitting of $^{57}Fe^{2+}$ in $FeCO_3$. Phys Rev B 32:3282–3284
Stanjek H, Häusler W (2000) Quantifizierung silikatischer Tonminerale im Textur- und Pulverpräparat mit MacClayFit. In: Hermanns Stengele R, Plötze M (eds) Berichte der DTTG 7, pp 256–265
Staubwasser M, von Blanckenburg F, Schoenberg R (2006) Iron isotopes in the early marine diagenetic iron cycle. Geology 34:629–632
Stoops G (1983) SEM and light microscopic observations of minerals in bog-ores of the Belgian Campine. Geoderma 30:179–186
Straub KL, Benz M, Schink B (2001) Iron metabolism in anoxic environments at near neutral pH. FEMS Microbiol Ecol 34:181–186
Teutsch N, von Gunten U, Porcelli D, Cirpka OA, Halliday AN (2005) Adsorption as a cause for iron isotope fractionation in reduced groundwater. Geochim Cosmochim Acta 69:4175–4185
Teutsch N, Schmid M, Muller B, Halliday AN, Burgmann H, Wehrli B (2009) Large iron isotope fractionation at the oxic–anoxic boundary in Lake Nyos. Earth Planet Sci Lett 285:52–60
Thompson A, Chadwick OA, Rancourt DG, Chorover J (2006) Iron-oxide crystallinity increases during soil redox oscillations. Geochim Cosmochim Acta 70:1710–1727
Thompson A, Ruiz J, Chadwick OA, Titus M, Chorover J (2007) Rayleigh fractionation of iron isotopes during pedogenesis along a climate sequence of Hawaiian basalt. Chemical Geology 238:72–83
Thompson A, Rancourt DG, Chadwick OA, Chorover J (2011) Iron solid-phase differentiation along a redox gradient in basaltic soils. Geochim Cosmochim Acta 75:119–133
van der Zee C, Roberts DR, Rancourt DG, Slomp CP (2003) Nanogoethite is the dominant reactive oxyhydroxide phase in lake and marine sediments. Geology 31:993–996
van der Zee C, Slomp CP, Rancourt DG, De Lange GJ, Van Raaphorst W (2005) A Mössbauer spectroscopic study of the iron redox transition in eastern Mediterranean sediments. Geochim Cosmochim Acta 69:441–453
Weber KA, Achenbach LA, Coates JD (2006) Microorganisms pumping iron: anaerobic microbial iron oxidation and reduction. Nat Rev Microbiol 4:752–764
Wei SY, Liu F, Feng XH, Tan WF, Koopal LK (2011) Formation and transformation of iron oxide–kaolinite associations in the presence of iron(II). Soil Sci Soc Am J 75:45–55
Weyer S, Schwieters J (2003) High precision Fe isotope measurements with high mass resolution MC-ICPMS. Int J Mass Spectrom 226:355–368
Weyer S, Anbar AD, Brey GP, Munker C, Mezger K, Woodland AB (2005) Iron isotope fractionation during planetary differentiation. Earth Planet Sci Lett 240:251–264
Wiederhold JG (2006) Iron isotope fractionation in soils—from phenomena to process identification. PhD thesis. Diss. ETH no. 16849, 148 p. Zürich, Switzerland
Wiederhold JG, Teutsch N, Kraemer SM, Halliday AN, Kretzschmar R (2007a) Iron isotope fractionation during pedogenesis in redoximorphic soils. Soil Sci Soc Am J 71:1840–1850
Wiederhold JG, Teutsch N, Kraemer SM, Halliday AN, Kretzschmar R (2007b) Iron isotope fractionation in oxic soils by mineral weathering and podzolisation. Geochim Cosmochim Acta 71:5821–5833
Wiesli RA, Beard BL, Johnson CM (2004) Experimental determination of Fe isotope fractionation between aqueous Fe(II), siderite and "green rust" in abiotic systems. Chem Geol 211:343–362
Williams AGB, Scherer MM (2004) Spectroscopic evidence for Fe (II)–Fe(III) electron transfer at the iron oxide-water interface. Environ Sci Technol 38:4782–4790
Williams HM, Peslier AH, McCammon C, Halliday AN, Levasseur S, Teutsch N, Burg JP (2005) Systematic iron isotope variations in mantle rocks and minerals: the effects of partial melting and oxygen fugacity. Earth Planet Sci Lett 235:435–452
WRB, IUSS Working Group (2006) World reference base for soil resources 2006, 2nd edition, World Soil Resources Reports No. 103. FAO, Rome
Zachara JM, Kukkadapu RK, Fredrickson JK, Gorby YA, Smith SC (2002) Biomineralization of poorly crystalline Fe(III) oxides by dissimilatory metal reducing bacteria (DMRB). Geomicrobiol J 19:179–207